




# Synthesis of homogeneous styrenic pyridine resin (LSL-030-bd) and its application to the separation of uranium and molybdenum

Yukai Peng<sup>1</sup> · Jiahui Li<sup>2</sup> · Jingfang Xue<sup>1</sup> · Hao Jin<sup>1</sup> · Yu Zeng<sup>1</sup> · Wei Zhao<sup>1</sup> · Xuebin Su<sup>3</sup> · Rong Hua<sup>1</sup> 

Received: 21 May 2024 / Accepted: 6 August 2024  
© Akadémiai Kiadó, Budapest, Hungary 2024

## Abstract

This paper synthesized a styrypyridine (LSL-030-bd) resin with small particle size and uniform distribution to recover molybdenum resources leached during neutral in-situ leaching of uranium. The batch experiment results show that the LSL-030-bd ion exchange resin produced had the highest U(VI) adsorption capacity at pH 7.0, reaching 187.20 mg·g<sup>-1</sup>. At pH 3.0, LSL-030-bd resin adsorbed 180.17 mg·g<sup>-1</sup> of Mo(VI). At pH 7.0, the resin exhibited the highest separation coefficient for uranium and molybdenum, with a KD value of 9.08. The resin's adsorption of U(VI) is a spontaneous endothermic process involving monolayer adsorption that combines physical and chemical adsorption. The adsorption of Mo(VI) by the resin is an exothermic process that is not spontaneous. It involves monomolecular layer adsorption with hydrogen bonding as the primary chemical force. By desorbing molybdenum with NH<sub>4</sub>SCN, followed by utilizing a mixed solution of NH<sub>4</sub>HCO<sub>3</sub> and (NH<sub>4</sub>)<sub>2</sub>CO<sub>3</sub> to desorb uranium, a step-by-step desorption process may be achieved to separate and purify uranium and molybdenum.

**Keywords** LSL-030-bd resin · Ion exchange · Uranium · Molybdenum separation · Adsorption · Desorption

## Introduction

Uranium is a crucial strategic resource for China's economic construction and national defense security [1]. However, China's uranium deposits are widely distributed, feature low quality, and are generally found in association with other minerals [2]. The uranium hydrometallurgical process has evolved to handle uranium ore that has shifted from being shallowly buried, high-grade, as well as consisting of a single component, to being deeply buried, low-grade, yet composed of complicated components. The international

uranium price has rebounded in recent years, while the high cost of uranium mining, attributed to deep burial and low grade, poses challenges for firms to achieve viable mining for most low-quality deposits [3]. Molybdenum is frequently found in natural uranium ore in minerals including uranium-molybdenite, uranium-molybdenum-gold-silver ore, and uranium-phosphorite [4–6]. Molybdenum is extensively utilized in several industries, like chemical, nuclear, aerospace, manufacturing, and electronics, owing to its exceptional physical and chemical characteristics. It is a crucial strategic commodity for national security and economic progress, with a price ten times higher than that of natural uranium on the market. The key to achieving strategic resource production and storage growth is the advancement of uranium-molybdenum separation and recycling technology, which can lower the cost of natural uranium production [7, 8].

Solvent extraction is typically employed for separating uranium and molybdenum in solution systems with high concentrations; instead, ion exchange is a more cost-effective and practical option for low concentrations [9, 10]. Over the years of monitoring uranium leach solution components, it has been observed that regardless of the leaching process employed, molybdenum is partially dissolved into

✉ Xuebin Su  
suxuebin1968@163.com

✉ Rong Hua  
huarong80@126.com

<sup>1</sup> National Key Laboratory of Uranium Resource Exploration-Mining and Nuclear Remote Sensing, East China University of Technology, Nanchang 330013, Jiangxi, China

<sup>2</sup> CGNPC Uranium Resources Co., Ltd., Beijing 100029, China

<sup>3</sup> China National Uranium Corporation Limited, Beijing 100013, China

the leach solution during uranium dissolution. This results in a high uranium background with a low concentration of molybdenum (1–10 ppm) [11]. Therefore, utilizing an ion exchange separation and enrichment process is a more logical option. An extensive study has been conducted on the recovery of molybdenum metal using the ion exchange method, both domestically and internationally, with notable contributions from researchers such as Wang Lei et al. [12] used Ls-36y resin for the extraction of molybdenum from acidic wastewater in Guo Shuanghua. [13] used D314 ion exchange resin to extract molybdenum from molybdenum precipitation masterbatch; Pedro Orrego et al. [14] utilized two resins, L-MP62 and M43, for the extraction of uranium and molybdenum from copper leach solution.

In this paper, homogeneous styrene-based pyridine resin (LSL-030-bd) was synthesized in accordance with the separation and enrichment of low-enriched molybdenum against the backdrop of high uranium, as well as the adsorption properties of the material on uranium and molybdenum were investigated by combining the static and dynamic modes to obtain the separation coefficients of uranium and molybdenum, the resin under the external environmental conditions of neutral uranium mining and the microstructural characterization of the material before and after adsorption was carried out by large-scale instruments, such as SEM-EDS, FT-IR, XPS, alongside the adsorption mechanism was investigated by combining thermodynamic and kinetic fitting; a complete set of separation and recovery technologies for uranium and molybdenum under the conditions of neutral uranium extraction by ground leaching has been initially formed.

## Materials and methods

### Materials

Anhydrous sodium carbonate, 2,4-dinitrophenol, anhydrous ethanol, styrene, divinylbenzene, dibenzoyl peroxide, polypropylene glycol, sodium chloride, carboxymethylcellulose, azidoarsenic acid III, copper sulfate, potassium thiocyanate, and ammonium thiocyanate were analytically AR, 99.9% ammonium molybdate tetrahydrate, and the water used for experimental studies was deionized water.

### Instrumentation

GEN10S UV–Vis Visible Spectrophotometer, Thermo Fisher, USA; NNS-450 Scanning Electron Microscope, Philips FEI, The Netherlands; Nicolet-460 Infrared Spectrometer, Thermo Fisher, USA; Thermo K-Alpha + X-Ray Photoelectron Spectroscopy, Thermo Fisher, USA. Thermo

K-Alpha + X-Ray Photoelectron Spectrometer, Thermo Fisher, USA.

## Synthesis of pyridine-functionalized ion exchange resin (LSL-030-bd)

### Preparation of a homogeneous resin skeleton (white balls)

The resin skeleton (white ball) utilized in this study was a polystyrene-divinylbenzene homogeneous granular benzene ball. The initial mixture material was prepared by combining and reacting styrene, divinylbenzene, the initiator BPO (dibenzoyl peroxide) and the porogenic agent (polypropylene glycol), the second mixture material was obtained by mixing the sodium chloride solution and carboxymethylcellulose (for the aqueous-phase solution having a high ionic strength and organics, which is convenient for the fine-grained resin skeleton to be Generation); the first mixture of materials and the second mixture of materials using the tube injection method to add the first mixture of materials to the second mixture of materials contained in a three-necked flask mixing crosslinking polymerization reaction, the reaction is completed, filtration, the resulting solid material washed and air-drying, and then sieved, to obtain the particle size of 0.3–0.4 mm polystyrene—divinylbenzene polymer, schematic diagram. Figure 1 displays the schematic diagram, whereas Fig. 2 illustrates the steps.

### Preparation of chlorine spheres (LSL)

The white ball and chloromethyl ether were mixed in a 1:5 mass ratio. A catalyst, 0.2 times the mass of the white ball in zinc chloride, was added. The chloromethylation reaction took place at 50 °C. After pretreatment with sodium hydroxide and hydrochloric acid, the resulting chlorine ball was washed with deionized water. The procedure is illustrated in Fig. 3.

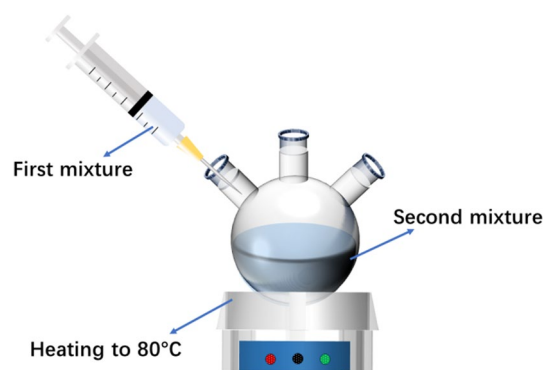
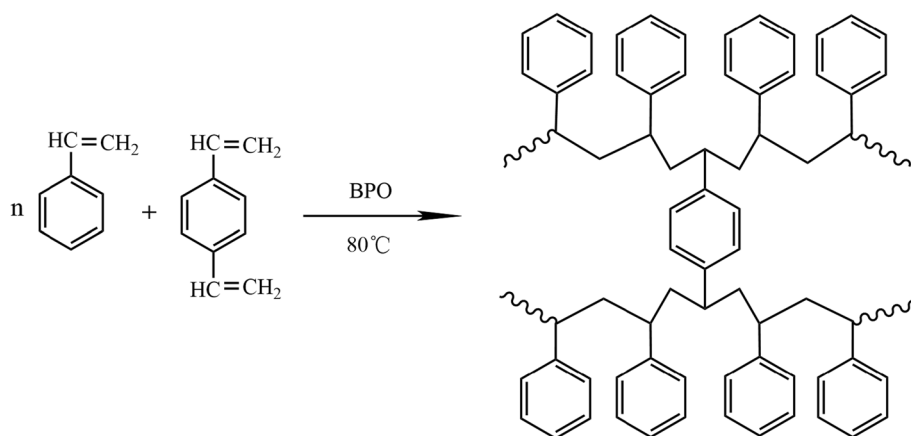
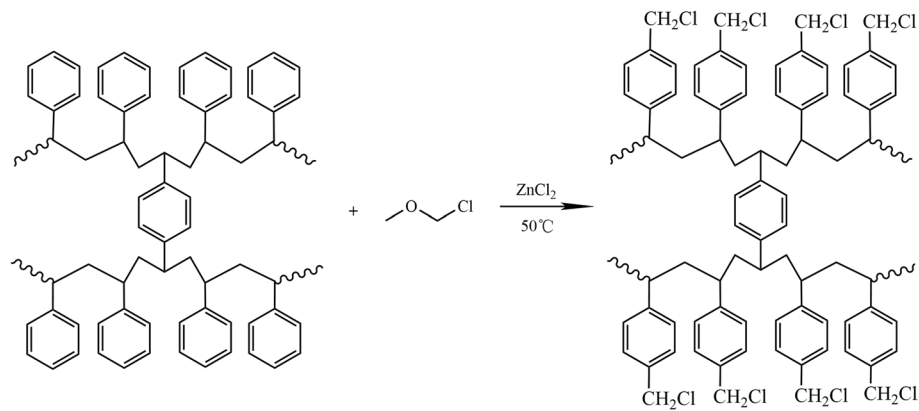
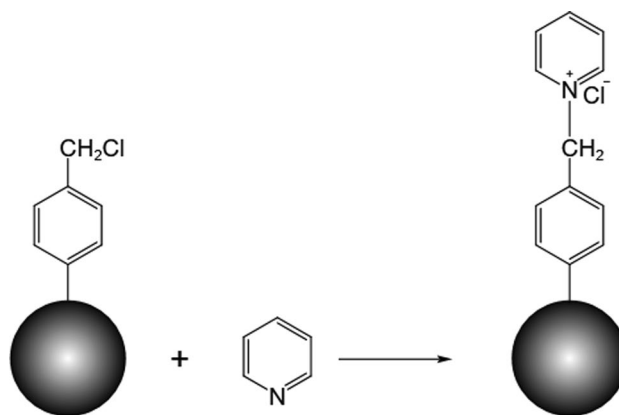


Fig. 1 Schematic diagram of white ball synthesis

**Fig. 2** Preparation of the resin skeleton (white ball)**Fig. 3** Preparation of chlorine spheres

### Functionalization of LSL-030-bd resin

50 mL of deionized water and 20 g of chlorine spheres (LSL) were combined in a three-necked flask and agitated at 90 °C for 6 h. Subsequently, 10 g of pyridine with a mass concentration of 30% were introduced, and the reaction proceeded at 60 °C for 6 h. The pyridine-functionalized anion-exchange resin (LSL-030-bd) was washed with acetone, ethanol, and deionized water many times after the reaction to remove excess impurities. It was then dried at 60 °C. The resin was repeatedly washed with acetone, ethanol, and deionized water to ensure the removal of excess impurities, such as possible unreacted monomers, solvents, catalyst residues, inorganic salts, or other insoluble substances; improve resin quality and performance; and then dried at 60 °C for future use. Figure 4 illustrates the synthesis process.

**Fig. 4** Synthesis of LSL-030-bd resin

### Transformation of Resins Activation

20 g of LSL-030-bd resin was taken in a 400 mL beaker, 100 mL of 1 mol·L<sup>-1</sup> NaOH solution was added, and it was left to stand for 4 h. After that, it was washed with deionized water until neutral, and 100 mL of 1 mol·L<sup>-1</sup> nitric acid was immersed for 4 h. Deionized water was washed until

neutral, and 250 mL of a 10% mass fraction of Na<sub>2</sub>CO<sub>3</sub> were immersed, washed, filtered, and dried for spare use.

### Preparation of U and Mo working solution

1. Uranium adsorption reserve solution (1 g·L<sup>-1</sup>): Weigh 1.1792 g of U<sub>3</sub>O<sub>8</sub> in a 250 mL beaker using an analytical balance. Add 20 mL of aqua regia and heat until the

solid dissolves completely. Evaporate until viscous, cool to room temperature, then add 150 mL of a mixed solution containing  $20 \text{ g}\cdot\text{L}^{-1} \text{Na}_2\text{CO}_3$  and  $10 \text{ g}\cdot\text{L}^{-1} \text{NaHCO}_3$ . Finally, add deionized water to a 1 L volumetric flask to set the volume.

2. Molybdenum adsorption reserve solution ( $1 \text{ g}\cdot\text{L}^{-1}$ ):  $1.8391 \text{ g} (\text{NH}_4)_6\text{Mo}_7\text{O}_{24}\cdot 4\text{H}_2\text{O}$  was accurately weighed in a 50 mL beaker with an analytical balance, and then added to 20 mL of deionized water to dissolve completely, and then fixed with deionized water in a 1 L volumetric flask.

## Results and discussion

### Characterization of synthetic resins (elemental analysis, infrared)

#### Scanning electron microscopy and energy spectroscopy (SEM–EDS) analysis

SEM–EDS was utilized to examine the morphology of LSL-030-bd resin, including white balls, chlorine balls, and resin, before and after transformation in the synthesis process. The resin's holomorphic images are displayed in Fig. 5a, c, e, g. The particle radius of the resin, whether in its skeleton form or following pyridine functionalization, is relatively uniform, with a radius of 0.3–0.4 mm maintained for the resin skeleton. Upon modification and activation, the resin skeleton swells and stretches, resulting in a radius of approximately 0.5 mm., which indicates that the new resin synthesized particles are smaller and the particle size homogeneity is better, which ensures that the contact area of the resin is more homogeneous and is conducive to the stability of the resin's overall function. From the surface microstructure of the resin as shown in Fig. 5b, d, f, h. Figure 5a, b, c, d shows that the surface of the white and chlorine spheres is rougher and tighter than the surface, and there are only a few fine particles on the surface. In Fig. 5f, h, the surface of the resin has been grafted with a large number of groups after transformation, and these groups show irregular and loose stacking of flakes on the surface of the resin, which signifies that the ion exchange resin has already possessed a large contact area.

The microcellular elemental analysis results from Table 1 show successful outcomes in resin, skeleton synthesis, and chlorine sphere preparation. Particularly, the significant increase in chlorine root content during chlorine sphere preparation suggests a high accessibility to pyridine functional groups. The change in chlorine root content before and after transformation indicates successful grafting of pyridine groups onto the resin skeleton during pyridine functionalization. The decrease in chlorine root content

post-transformation accurately reflects the resin's exchange capacity, predicting a high exchange capacity. The reduction in chlorine content post-transformation demonstrates the resin's exchange capacity, suggesting an increase in its ability to exchange ions.

### Fourier transform infrared spectroscopy (FT-IR) characterization of resins

Figure 6 shows broad peaks at  $3382 \text{ cm}^{-1}$  and  $1631 \text{ cm}^{-1}$ , attributed to the stretching and bending vibrations of the aqueous hydroxyl group. Vibration peaks of the C–H bond are observed at  $2928 \text{ cm}^{-1}$  and  $2851 \text{ cm}^{-1}$  [15], while the peak at  $1452 \text{ cm}^{-1}$  corresponds to the C=O stretching vibration, indicating the presence of carbonic acid in the resin skeleton [15]. The presence of the C=N absorption peak at  $1540 \text{ cm}^{-1}$  confirms the successful integration of pyridine into the resin structure, demonstrating the effective functionalization of the resin [16]. The  $823 \text{ cm}^{-1}$  peak represents the C–H outward bending vibration of benzene 1, 4-disubstitution, whereas the  $695 \text{ cm}^{-1}$  peak corresponds to the C–H outward bending vibration of benzene, providing structural information on the skeleton of styrene resin [15].

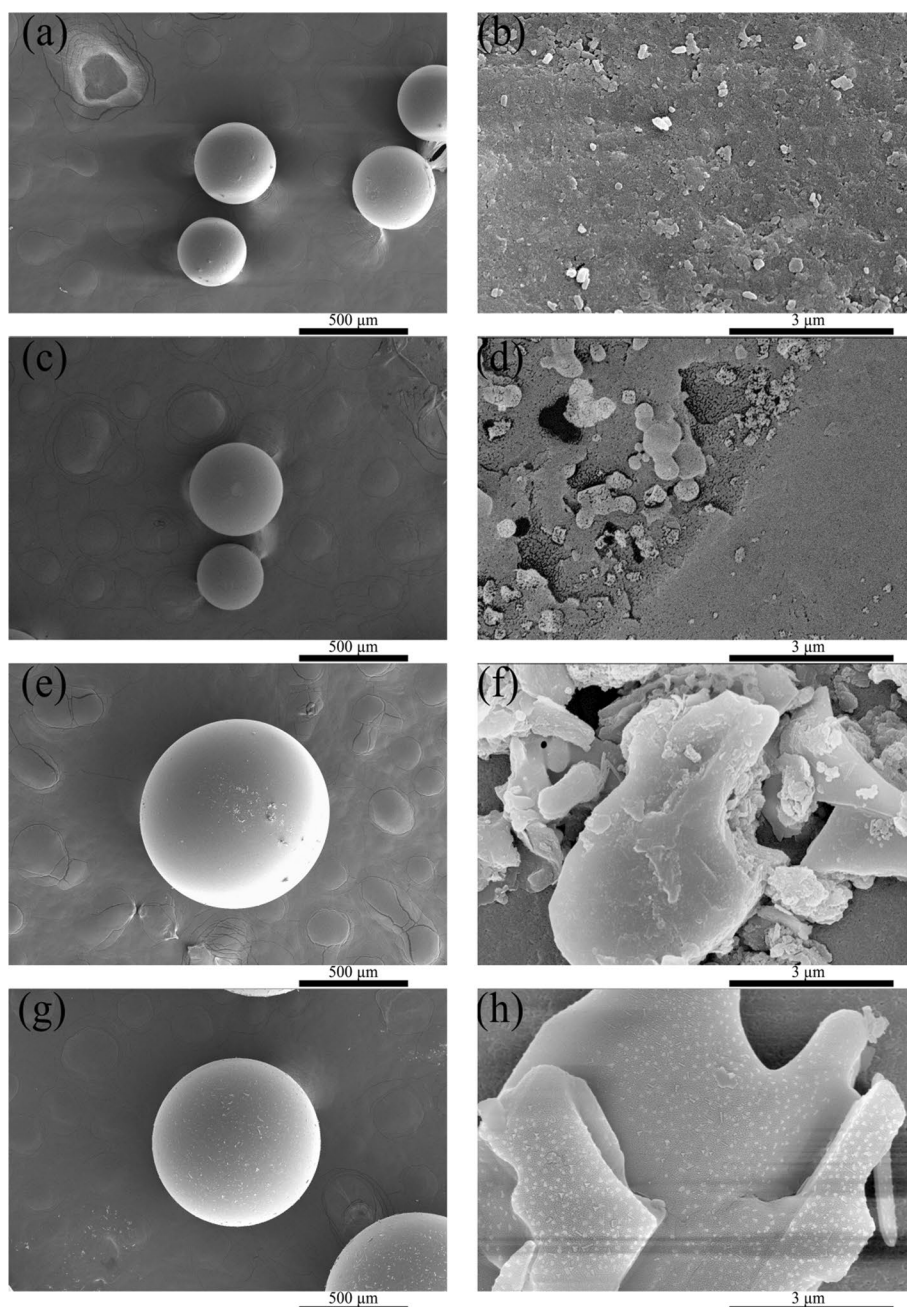
### Effect of pH on resin adsorption of uranium and molybdenum

Figure 7 illustrates the primary chemical forms of uranium and molybdenum in various pH solutions [17]. In carbonate solutions, the morphology of uranium and molybdenum is more intricate [18]. Considering the current neutral uranium mining pH range of 6.5–8.0 [19], it can be initially inferred that the solution predominantly consists of ions such as  $(\text{UO}_2)_2\text{CO}_3(\text{OH})_3^-$ ,  $\text{UO}_2^{2+}$  and  $\text{MoO}_4^{2-}$ .

Measure precisely  $0.02 \pm 0.0002 \text{ g}$  of LSL-030-bd ion exchange resin and place it in a 25 mL sample bottle. Then, the pH value is adjusted from 2.0 to 10.0 with dilute  $\text{H}_2\text{SO}_4$ ,  $\text{Na}_2\text{CO}_3$  and  $\text{NaOH}$  solutions, add 20 mL of  $300 \text{ mg}\cdot\text{L}^{-1}$  of a uranium and molybdenum standard solution with pH values ranging from 2.0 to 10.0 sequentially. Place the container in a constant-temperature oscillation box and oscillate it for 24 h at a temperature of  $25 \text{ }^\circ\text{C}$ . The liquid portion was collected to determine the levels of uranium and molybdenum that were still present in the solution after adsorption, as well as the adsorbance of uranium and molybdenum that had been adsorbed.

Figure 8 illustrates how its adsorption capacity increases with pH 2–4. Figure 7 shows that uranium exists mainly in the form of  $\text{UO}_2^{2+}$ . The adsorption of the resins increases due to the ion exchange of complex anions generated by  $\text{SO}_4^{2-}$  and  $\text{UO}_2^{2+}$ , as well as the hydrogen bonding of cations. The maximum value was  $133.75 \text{ mg}\cdot\text{g}^{-1}$  at pH 4.0. The ability of uranyl ions to bind to carbonate varied with pH.

**Fig. 5** SEM images of LSL-030-bd. White ball (a, b). Chlorine ball (c, d). Pre-transition (e, f). Post-transition (g, h)



**Table 1** The element content of LSL-030-bd before and after adsorption

elemental	white ball		chloromethane		Pre-transition		post-transition	
	Wt %	At %	Wt %	At %	Wt %	At %	Wt %	At %
C	91.85	94.01	73.76	88.32	14.46	18.58	70.46	75.45
N	0	0	0	0	1.00	1.10	7.42	6.82
O	7.52	5.77	2.08	1.87	82.12	79.26	22.00	17.69
Cl	0.63	0.22	24.16	9.8	2.42	1.06	0.12	0.04

At pH 4–6, the binding capacity of the resin for uranyl ions decreases. Experimental studies and production practice have shown that this is due to the easy formation of alkaline

uranyl sulfate precipitate  $[(\text{UO}_2)_2\text{SO}_4(\text{OH})_2 \cdot 4\text{H}_2\text{O}]$  in the range of pH = 4~6 [20], which reacts as follows:

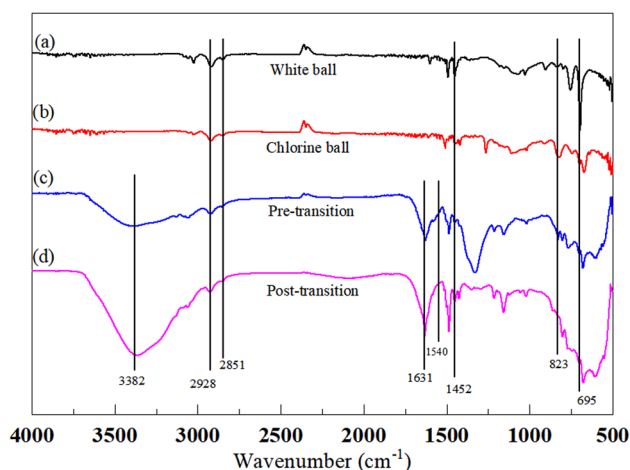
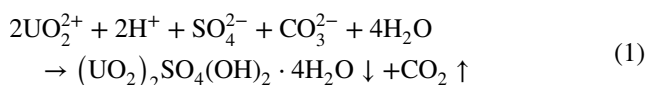
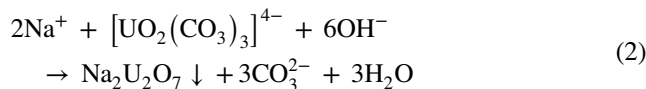


**Fig. 6** FT-IR spectra of **a** White ball, **b** Chlorine ball, **c** Pre-transition and **d** Post-transition)



Due to the hydrolysis and precipitation of uranyl ions, the total amount of uranyl ion complexes in the free state in the solution is reduced, and the concentration is lowered, so the total amount of uranyl ions that can be exchanged by the resin is reduced. When the pH value is between 7.0 and 10.0, the ability of the resin to adsorb uranium will first increase and then decrease. At pH 7–9.5, due to the presence of  $\text{CO}_3^{2-}$ , it changes to uranyl carbonate ion again, which is in line with the ion exchange process, and the adsorption capacity increases with the increase of pH, and it reaches the maximum at pH 9.5, which is  $168.82 \text{ mg}\cdot\text{g}^{-1}$ . However,

when the pH value is higher than 9.5, due to the increase in the concentration of  $\text{OH}^-$  ions, the uranyl carbonate ions in the solution decompose to produce the sodium diuranate precipitate with the following reaction formula [20]:



As sodium bicarbonate precipitation is produced by uranyl carbonate ions, the total number of uranyl ion complexes in the free state in the solution decreases along with their concentration. Consequently, the total amount of uranyl ions that the resin can exchange also decreases, preventing the resin from adsorbing uranium and decreasing their adsorption amount.

LSL-030-bd resin has superior adsorption efficacy for Mo in acidic conditions with a pH below 4. As per molybdenum's chemical form depicted in Fig. 7, the element is currently present as a complex cation ( $\text{MoO}_3(\text{H}_2\text{O})_3$ ), and its principal mode of adsorption in the resin mixture is hydrogen bonding. When the pH exceeds 4.0, Mo mostly exists as an anion ( $\text{MoO}_4^{2-}$ ) in the solution. Therefore, as the pH increases, the quantity of adsorption steadily diminishes. At a pH of 6.0 or higher, the resin's adsorption of Mo remained rather constant at  $30 \text{ mg}\cdot\text{g}^{-1}$ .

Based on the experimental data, specifically displayed in Fig. 9, the distribution coefficient of the resin for uranium and molybdenum in different pH settings. The separation factor of uranium and molybdenum is the largest when the pH is 7.0,  $\text{KD}=9.08$ . Under other conditions, the separation of uranium and molybdenum is not satisfactory. Combining the two processes of uranium production, the pH of  $\text{CO}_2 + \text{O}_2$  neutral leaching uranium is usually between 6.8 and 9 [1], and the resin has the largest separation coefficient of uranium and molybdenum at pH=7.0. It is finally

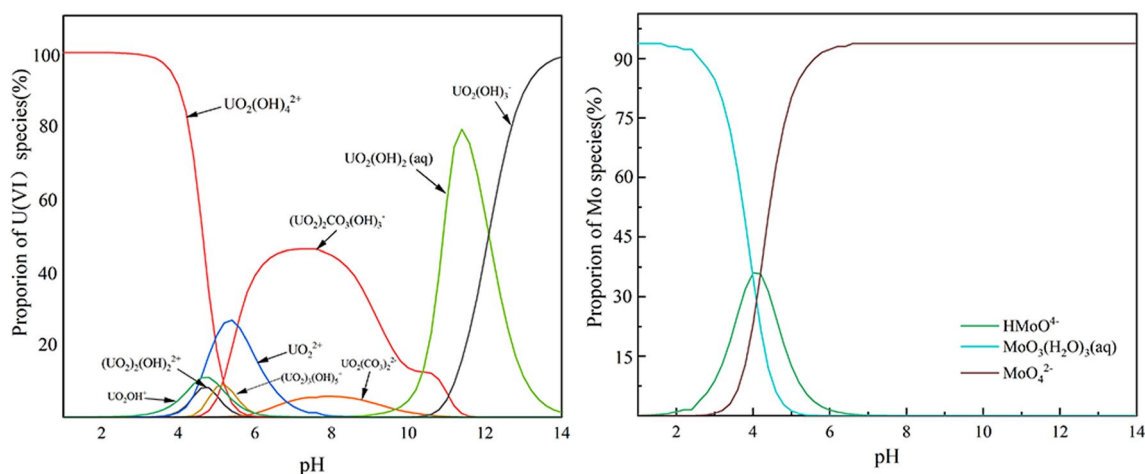


**Fig. 7** Speciation diagram of U and Mo in different pH solutions

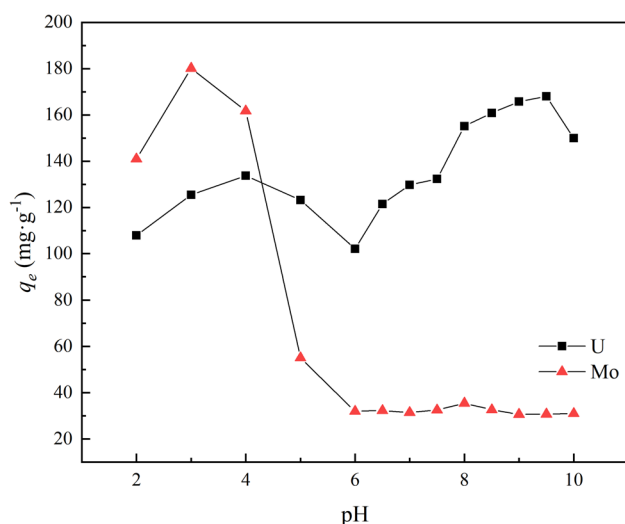


**Fig. 8** Effect of solution acidity on the adsorption of LSL-030-bd resin

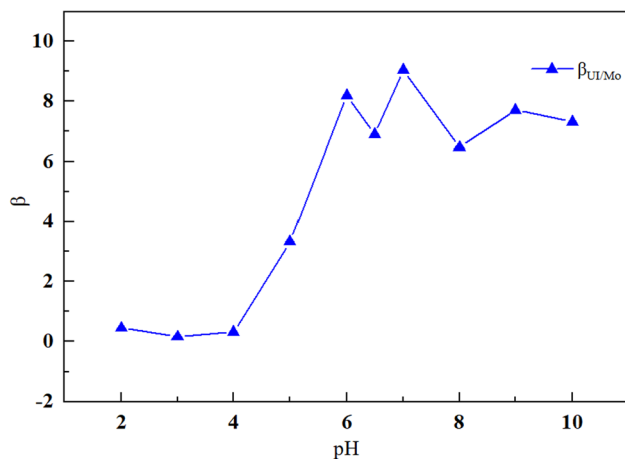


**Fig. 9** The separation coefficient between uranium and molybdenum

determined that the adsorbent material has some prospects for uranium and molybdenum separation in  $\text{CO}_2 + \text{O}_2$  neutral in-situ leaching of uranium, and it is selected to be utilized at a pH of 7.0 in the current investigation.

### Adsorption isotherm studies

Measure precisely  $0.02 \pm 0.0002$  g of LSL-030-bd ion exchange resin and place it in a 25 mL sample bottle. Add 20 mL of a uranium and molybdenum standard solution with a pH value of 7.0 in turn. Place the sample bottle in a constant-temperature oscillation box and oscillate it for a duration of 24 h at a temperature of 25 °C.

At a pH of 7.0, altering the initial concentration of the solution results in a corresponding modification of the resin's

adsorption capacity. An experiment was conducted to examine the adsorption of uranium and molybdenum by the resin at a pH of 7.0. Its results are displayed in Fig. 10.

When the initial concentration of the uranium solution is below  $200 \text{ mg}\cdot\text{L}^{-1}$ , its adsorption capacity increases significantly as the initial concentration of the solution increases. However, when the initial concentration exceeds  $200 \text{ mg}\cdot\text{L}^{-1}$ , the adsorption capacity basically reaches a saturation point, specifically at  $178.09 \text{ mg}\cdot\text{g}^{-1}$ . At a pH of 7.0, the LSL-030-bd resin exhibits low adsorption of molybdenum, with an adsorption capacity of  $34.54 \text{ mg}\cdot\text{g}^{-1}$ . The adsorption capacity shows a slight increase as the initial concentration of molybdenum increases. At an initial concentration of  $150 \text{ mg}\cdot\text{L}^{-1}$ , the resin reached its saturation point with an adsorption capacity of  $34.54 \text{ mg}\cdot\text{g}^{-1}$ . As the initial concentration increased, the adsorption capacity slightly increased as well, reaching  $43.06 \text{ mg}\cdot\text{g}^{-1}$  at an initial concentration of  $350 \text{ mg}\cdot\text{L}^{-1}$ .

The data was fitted employing the Langmuir and Freundlich isothermal adsorption models [21], and the results can be shown in Fig. 11.

Based on the Langmuir and Freundlich isothermal adsorption models shown in Fig. 11, it is evident that the adsorption of uranium by LSL-030-bd resin aligns more closely with the Langmuir isothermal adsorption model ( $R_{1L}^2 = 0.99478$ ) than the Freundlich isothermal adsorption model ( $R_{1F}^2 = 0.7613$ ). This suggests that the adsorption process involves the formation of a monomolecular layer. Additionally, it indicates that the functional groups of the adsorbent materials, synthesized through a two-step process, are primarily attached to the resin's surface during the functionalized grafting process. The resin's adsorption process for molybdenum is more accurately described by the Langmuir isothermal adsorption model, suggesting that the

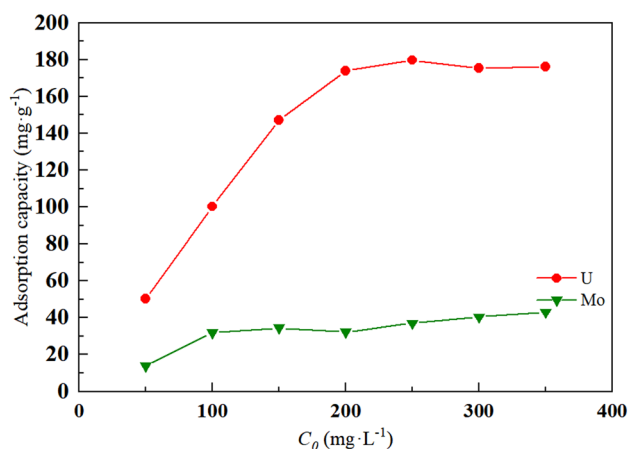


**Fig. 10** Effect of initial concentration on the adsorption of uranium and molybdenum by LSL-030-bd resin

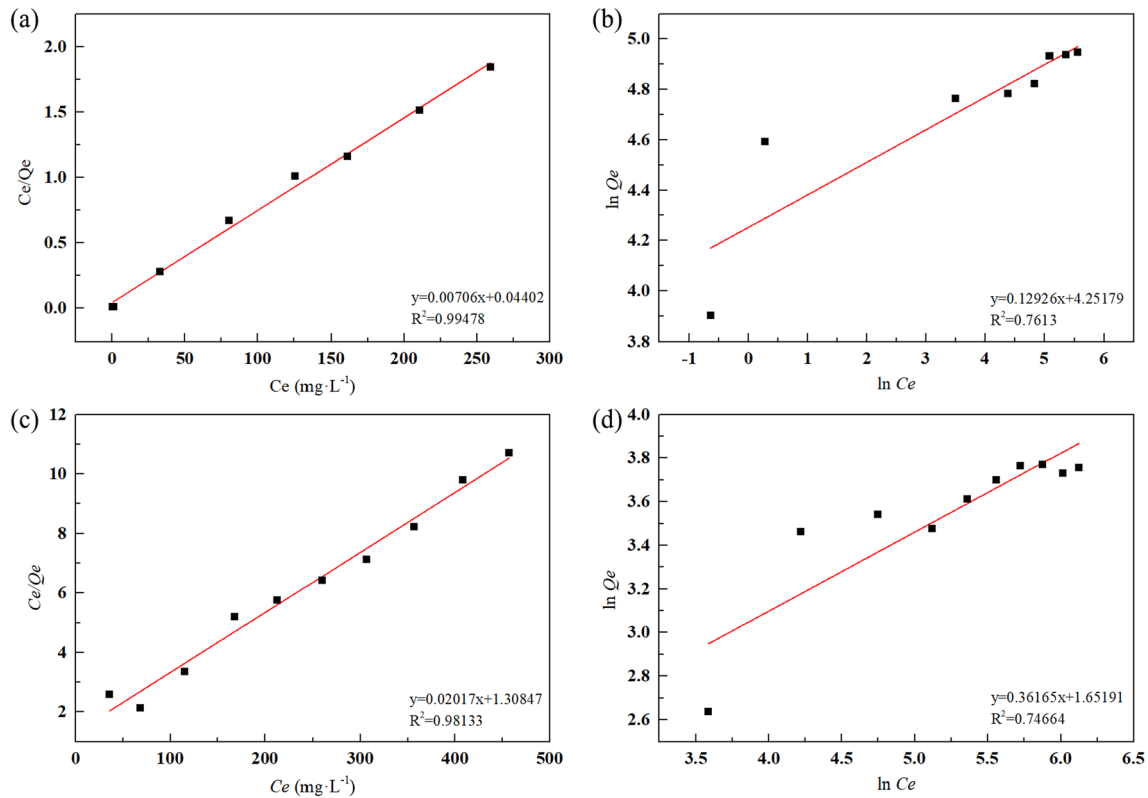


Fig. 11 Langmuir and Freundlich isothermal adsorption models for **a, b** uranium and **c, d** molybdenum

adsorption process involves the formation of monomolecular layer adsorption.

### Effect of resin dosage on the adsorption of LSL-030-bd resin

The adsorption rate of LSL-030-bd resin for uranium and molybdenum can be determined by examining the impact of resin dosage on adsorption. A total of 0.01, 0.02, 0.04, 0.06, 0.08, 0.1, 0.15, and 0.2 g of LSL-030-bd ion exchange resin were measured and placed into a 25 mL sample bottle. Subsequently, 20 mL of a pH 7.0 uranium and molybdenum standard solution with a concentration of  $200 \text{ mg}\cdot\text{L}^{-1}$  was added in a sequential manner. The sample bottle was then placed inside a constant temperature oscillation box and oscillated at a temperature of  $25 \text{ }^\circ\text{C}$  for a duration of 24 h.

According to the information provided in Fig. 12, it is evident that the LSL-030-bd resin exhibits effective adsorption of uranium. When the resin quantity is 40 mg, the uranium removal rate in the solution reaches 100%. Similarly, when the resin quantity is 150 mg, the adsorption of molybdenum reaches a state of equilibrium, resulting in a molybdenum removal rate of 22.76% in

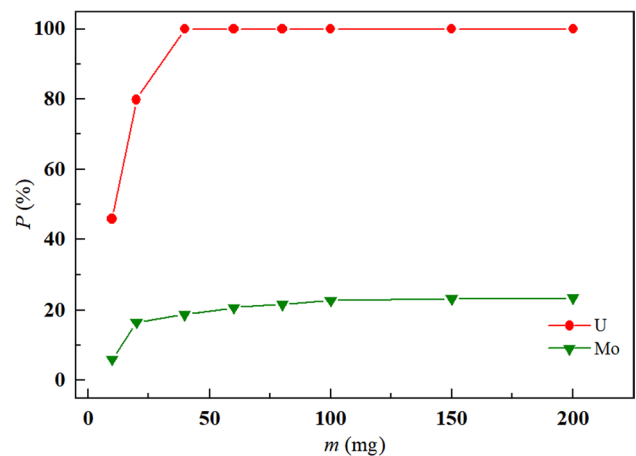


Fig. 12 Effect of resin dose on the adsorption of uranium and molybdenum by LSL-030-bd resin

the solution. To guarantee an adequate number of sites and capacity for uranium and molybdenum, a quantity of 100 mg of resin was employed for the subsequent adsorption kinetics tests.



## Adsorption kinetics studies

The effect of different times on the adsorption of LSL-030-bd resin was carried out at room temperature, pH

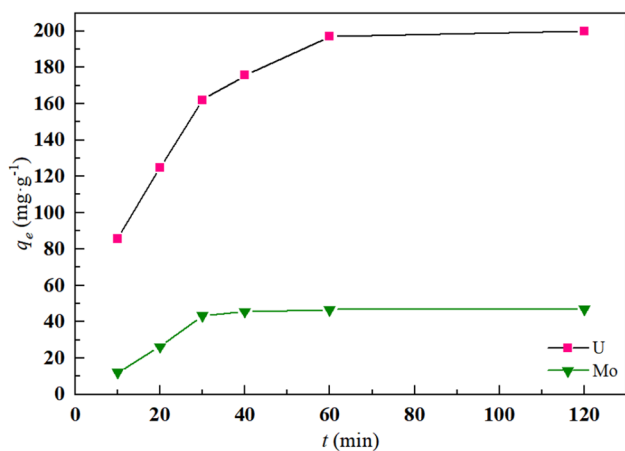


**Fig. 13** Effect of adsorption time on the adsorption of uranium and molybdenum by LSL-030-bd resin

7.0, a resin dosage of 0.1 g, and an initial concentration of  $200 \text{ mg}\cdot\text{L}^{-1}$ . The outcome is displayed in Fig. 13.

The adsorption of 0.1 g of LSL-030-bd resin for uranium reached equilibrium after 60 min, as shown in Fig. 13. It was able to hold  $196.99 \text{ mg}\cdot\text{g}^{-1}$ . The adsorption of the resin for molybdenum also basically reached equilibrium after 30 min, but the adsorption capacity was lower than that of uranium, measuring only  $43.36 \text{ mg}\cdot\text{g}^{-1}$ .

At 120 min, the amount of adsorption for molybdenum increased to  $47.02 \text{ mg}\cdot\text{g}^{-1}$ . The alteration was minor.

Following the kinetic model in Fig. 14, the adsorption of LSL-030-bd resin for uranium and molybdenum aligns better with the quasi-secondary kinetic model ( $R_U^2 = 0.99862$ ,  $R_{Mo}^2 = 0.9916$ ). The adsorption of LSL-030-bd resin for uranium follows quasi-primary kinetics ( $R_U^2 = 0.99382$ ), indicating that the adsorption process is influenced by both chemical action and physical adsorption. On the other hand, the quasi-primary kinetic model of the resin for molybdenum shows a low linear correlation coefficient, suggesting that the adsorption process of molybdenum by the resin is primarily governed by chemical chelation or hydrogen bonding.

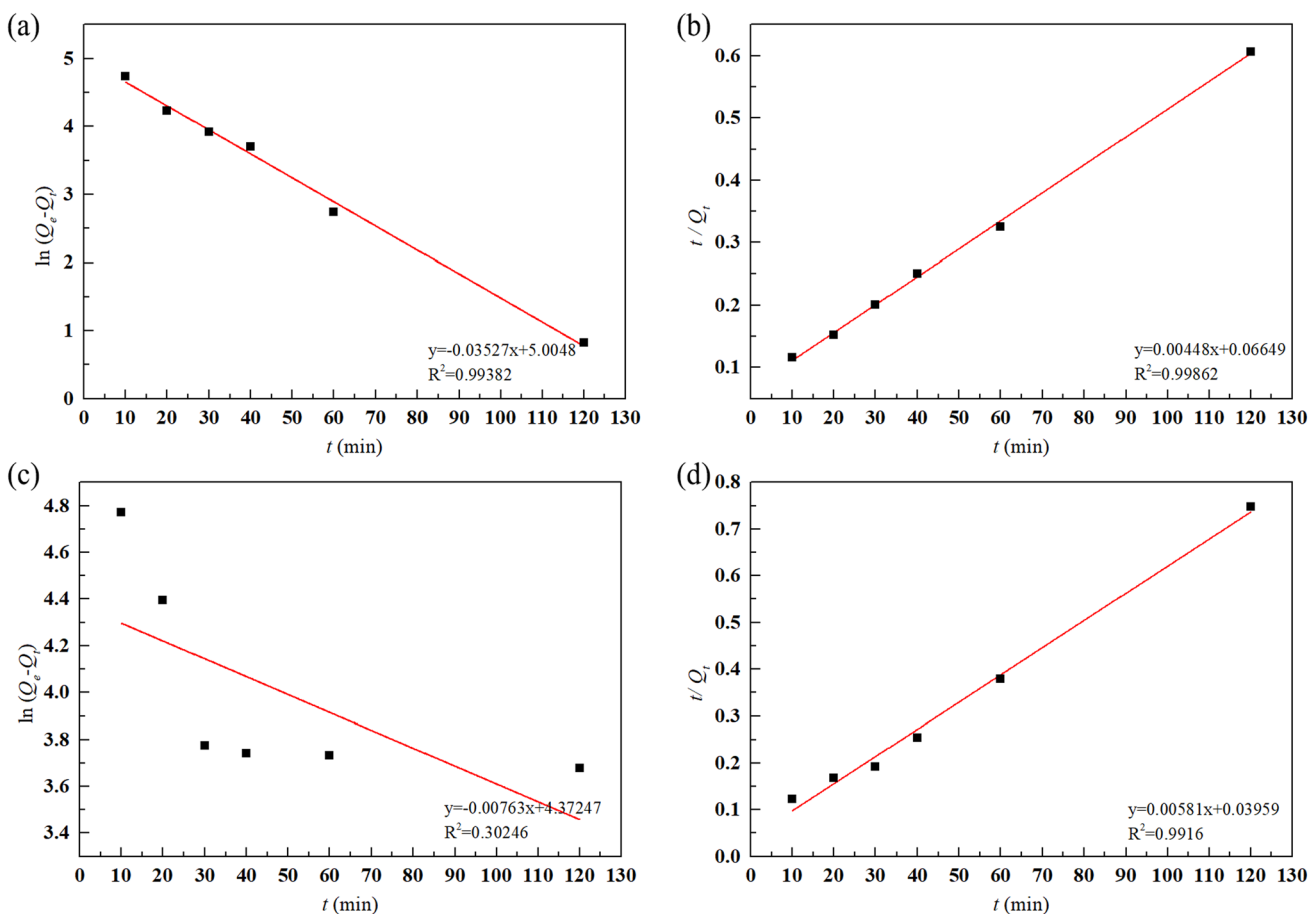


**Fig. 14** kinetic models of LSL-030-bd resin. **a, b** uranium, **c, d** molybdenum

## Thermodynamic studies

The effect of different temperatures on the adsorption of LSL-030-bd resin was carried out at a resin dosage of 0.02 g and an initial concentration of the solution of

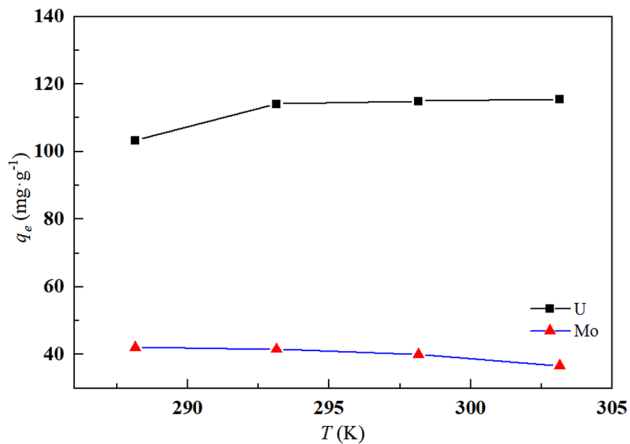


**Fig. 15** Effect of temperature on the adsorption of uranium and molybdenum by LSL-030-bd resin

200 mg·L<sup>-1</sup> with an oscillation time of 24 h. The results are shown in Fig. 15.

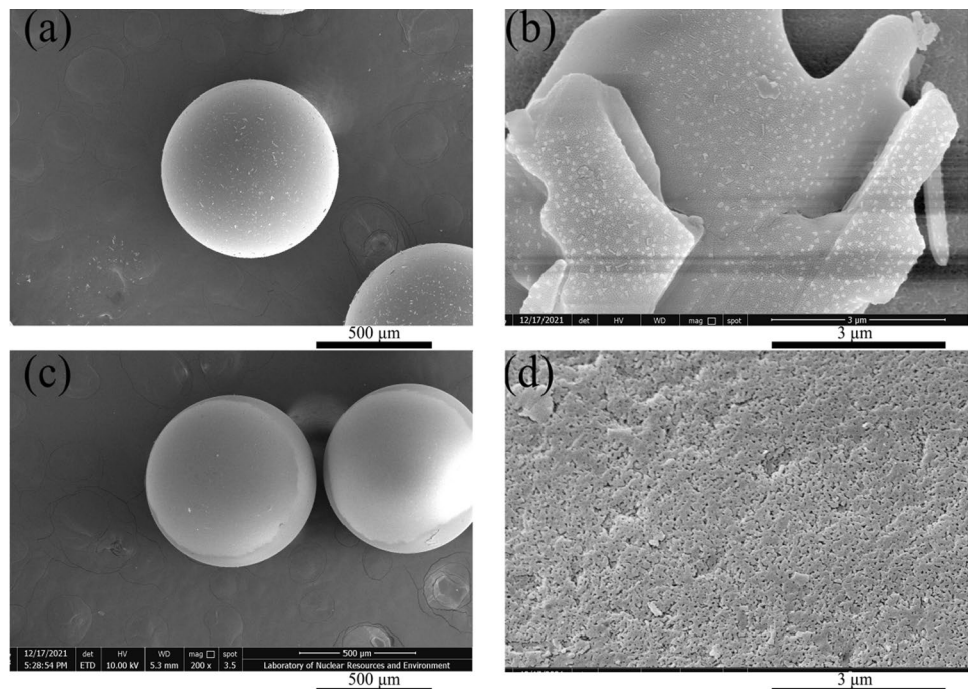
From Fig. 15, it is evident that as the temperature rises, the resin's adsorption capacity for U increases, while the adsorption capacity for Mo decreases. Considering practical production, it is more suitable to conduct the experiment under room temperature conditions (25 °C).

According to the information provided in Table 2, it is evident that within the temperature range of 288.15–303.15 K, the adsorption process of the resin for U(VI) exhibits  $\Delta H > 0$ ,  $\Delta S > 0$ , and  $\Delta G < 0$ . This indicates that the process absorbs heat [22], and an increase in temperature is beneficial for the resin's adsorption of U(VI). Additionally, entropy and disorder increase in the spontaneous process. On the other hand, the adsorption process of Mo(VI) is exothermic but not spontaneous, resulting in lower adsorption compared to U(VI). This aligns with the experimental findings, and the disorder decreases in this process.

**Table 2** Thermodynamic function value of LSL-030-bd resin

elemental	$\Delta H$ (kJ·mol <sup>-1</sup> ) <sup>-1</sup>	$\Delta S$ (kJ·mol <sup>-1</sup> ·K) <sup>-1</sup>	$\Delta G$			
			288.15 K	293.15 K	298.15 K	303.15 K
U	11.06	39.47	-0.298	-0.495	-0.693	-0.890
Mo	-1.980	-18.51	3.352	3.445	3.537	3.630

**Fig. 16** SEM images of LSL-030-30-bd. per-adsorption (a, b), post-adsorption (c, d)



## Scanning electron microscopy and energy spectroscopy (SEM–EDS) analysis

The SEM–EDS analysis was conducted to examine the morphology of LSL-030-bd resin prior to and after the adsorption of U(VI) and Mo(VI). Figure 16(c, d) illustrates the adsorption process of U(VI) and Mo(VI) by the

**Table 3** The element content of LSL-030-bd before and after adsorption

elemental	pre-adsorption		post-adsorption	
	Wt %	At %	Wt %	At %
C	70.46	75.45	43.61	77.72
N	7.42	6.82	2.36	3.61
o	22.00	17.69	9.25	12.37
Cl	0.12	0.04	0.80	0.49
U	0	0	1.78	0.16
Re	0	0	2.97	0.34
Mo	0	0	9.14	2.04
Au	–	–	30.08	3.27

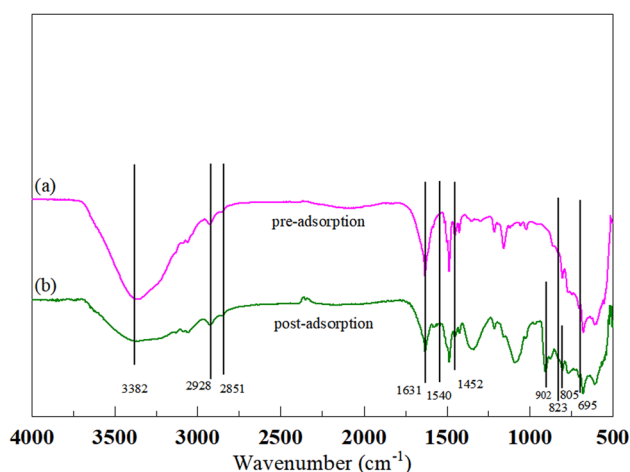
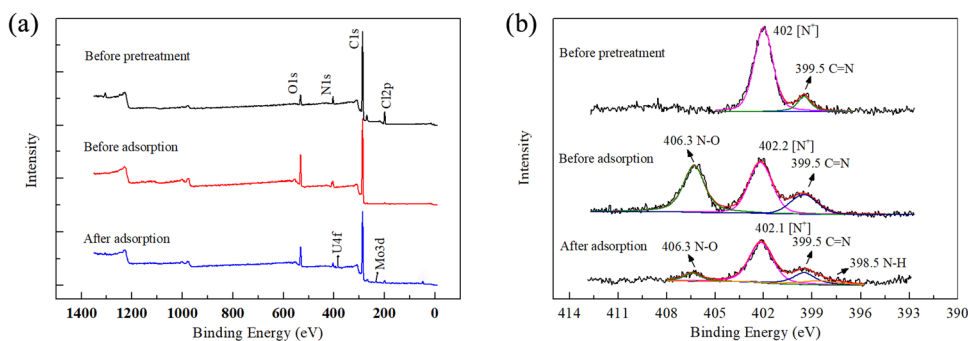


**Fig. 17** FT-IR spectra of LSL-030-bd before and after adsorption. pre-adsorption (a), post-adsorption (b)

**Fig. 18** Effect of adsorption time on the adsorption of uranium and molybdenum by LSL-030-bd resin



resin, revealing the presence of numerous network-like structures on its surface.

Characterizing the resin by scanning electron microscopy necessitates the application of a gold plating treatment. As a result, a significant quantity of gold (Au) is present on the resin's surface, and there is a partial overlap of Mo peaks and U peaks, so there is a certain degree of interference with the Mo elemental mass fraction. Specifically, the U(VI) mass fraction is 1.78% and the Mo(VI) mass fraction is 9.14%. This indicates that the LSL-030-bd resin successfully adsorbed U(VI) and Mo(VI). The successful adsorption of U(VI) and Mo(VI) by LSL-030-bd resin is indicated. The results are shown in Table 3.

## Fourier Transform Infrared Spectroscopy (FT-IR) Characterization

In Fig. 17, the symmetric vibration peak [23] at  $902\text{ cm}^{-1}$  corresponds to  $\text{UO}_2^{2+}$ , and the characteristic peak [17] at  $805\text{ cm}^{-1}$  corresponds to Mo(VI), which indicates that the resin successfully adsorbed U(VI) and Mo(VI) by ion exchange.

## X-ray photoelectron spectroscopy (XPS) analysis

The adsorption mechanism of LSL-030-bd was further analyzed by XPS analysis according to its constituent elements C, N, O, and Cl. In Fig. 18a, the Cl2p peak in LSL-030-bd resin disappeared after the transition, indicating that the resin was successfully converted from  $\text{Cl}^-$  type to  $\text{NO}_3^-$  or  $\text{CO}_3^{2-}$  type. After adsorption, two new peaks of  $381.7\text{ eV}$  (U4f) and  $232.65\text{ eV}$  (Mo3d) appeared, indicating the successful adsorption of uranium and molybdenum. To examine the interaction mechanism between the active site and uranium and molybdenum, high-resolution energy spectroscopy was introduced to analyze them. As depicted in Fig. 18b, the pre-transformation N1s spectrum can be divided into two separate peaks; the peak located at  $399.5\text{ eV}$  is the N in the incompletely reacted

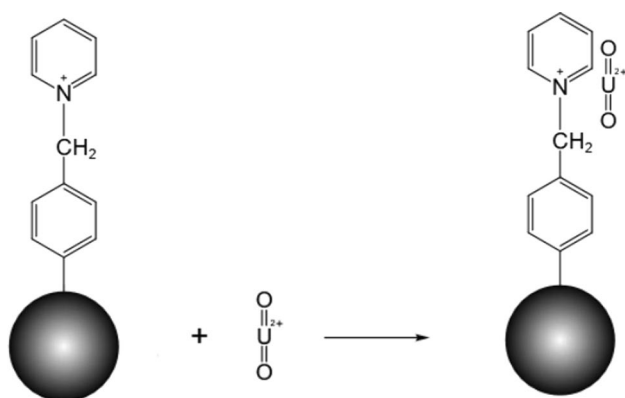


Fig. 19 Adsorption mechanism of LSL-030-bd towards U(VI)

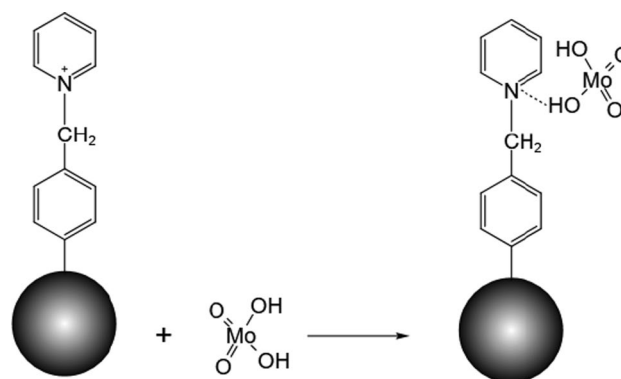


Fig. 21 Adsorption mechanism of LSL-030-bd towards Mo(VI)

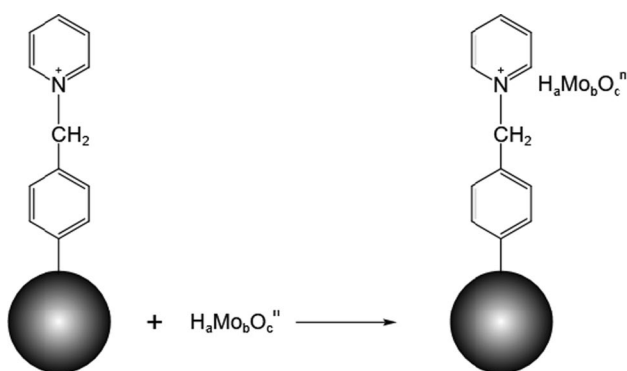


Fig. 20 Adsorption mechanism of LSL-030-bd towards Mo(VI)

pyridine ring, and 402 eV corresponds to the nitrogen atom with the protonated pyridine ( $C=N^+$ ) [16]. After the transition, a new peak at 406.3 eV appears, corresponding to the N–O bond in  $NO_3^-$ . Due to the electronegativity order:  $O > Cl > N > H > Mo > U$ , the N in the pyridine ring of the resin combines with the O of the  $CO_3^{2-}$  in  $NO_3^-$  or  $CO_3^{2-}$  to change from the N–Cl bond to the N–O bond, resulting in a change of the peak position of  $[N^+]$  from 402 to 402.2 eV. After adsorption, the peak of  $[N^+]$  changes from 402.2 to 402.1 eV, while a new peak at 398.5 eV and a weaker N–H appeared due to the presence of U(VI) in solution as  $UO_2(CO_3)_2^{2-}$  complex anion, which is due to the hydrogen bonding between N and Mo [16, 24].

In summary, it can be seen that the adsorption of uranium by LSL-030-bd resin is  $UO_2^{2+}$ . The complex anion combines with pyridine on the resin through ion exchange, and the process of molybdenum adsorption by LSL-030-bd resin has both ion exchange and chelation. The reaction mechanism is shown in the following Figs. 19, 20, and 21.

### Selection of conditions for stepwise desorption of uranium and molybdenum from resin

Previous tests have demonstrated that LSL-030-bd resin has the ability to adsorb both uranium and molybdenum. Therefore, it is suggested to separate these two elements by gradually desorbing them using various desorbent solutions.  $NH_4SCN$  and  $NH_4HCO_3 + (NH_4)_2CO_3$  mixed solutions were selected as desorbents after conducting initial experiments. The results are shown in Table 4.

According to the data in Table 4, when the concentration of  $NH_4SCN$  surpasses  $0.1 \text{ mol}\cdot\text{L}^{-1}$ , the desorption rate of molybdenum gradually increases from 92.72 to 92.83%. However, the desorption rate of uranium is only 3.33% when the concentration of  $NH_4SCN$  is  $0.1 \text{ mol}\cdot\text{L}^{-1}$ . On the other hand, when the concentration of  $NH_4HCO_3 + (NH_4)_2CO_3$  is  $1.5 \text{ mol}\cdot\text{L}^{-1}$ , the desorption rate of uranium reaches its highest point at 89.47%, while the desorption rate of molybdenum is 80.77%. So  $0.1 \text{ mol}\cdot\text{L}^{-1}$   $NH_4SCN$  was considered to desorb molybdenum first, followed by  $1.5 \text{ mol}\cdot\text{L}^{-1}$   $NH_4HCO_3 + (NH_4)_2CO_3$  to desorb uranium.

### Comparing the static and dynamic adsorption and desorption

Determination of the dynamic adsorption rate. Resin adsorption is divided into three processes: liquid film diffusion, particle diffusion, and chemical reaction [25], and the results obtained by fitting are shown in Table 5:

The adsorption and desorption of U follow the mechanism of particle diffusion. The dynamic adsorption laboratory instrument can handle a maximum flow rate of  $0.68 \text{ mL}\cdot\text{min}^{-1}$ . Thus, the flow rate for the dynamic adsorption experiment is chosen as  $0.5 \text{ mL}\cdot\text{min}^{-1}$ . The adsorption process of Mo is primarily governed by chemical reactions. The dynamic experimental equipment can accommodate a maximum flow rate of  $0.83 \text{ mL}\cdot\text{min}^{-1}$ . To enable complete

**Table 4** Desorption of uranium and molybdenum by two desorbing agents

serial number	NH <sub>4</sub> SCN concentration (mol·L <sup>-1</sup> )	Desorption rate (%)	NH <sub>4</sub> HCO <sub>3</sub> + (NH <sub>4</sub> ) <sub>2</sub> CO <sub>3</sub> Concentration (mol·L <sup>-1</sup> )	Desorption rate (%)
U-1	0.01	1.66	0.01	1.66
U-2	0.1	3.33	0.1	4.04
U-3	0.5	43.37	0.5	81.04
U-4	1.5	39.21	1.5	89.47
Mo-1	0.01	44.80	0.01	8.73
Mo-2	0.1	92.72	0.1	70.89
Mo-3	0.5	91.79	0.5	86.17
Mo-4	1.5	92.83	1.5	80.77

**Table 5** Study on adsorption process of LSL-030-bd resin

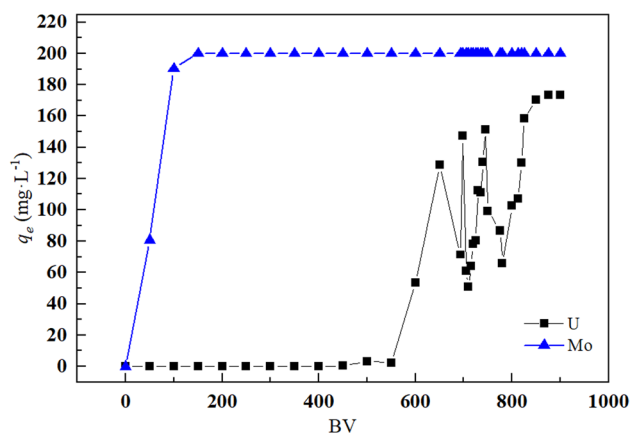
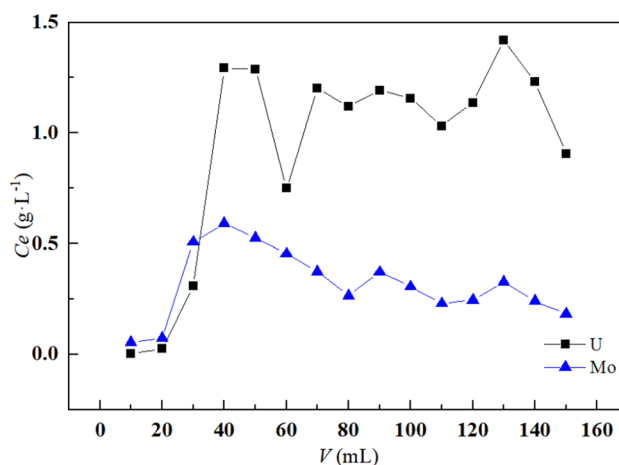
elemental	U			Mo		
	liquid film diffusion	particle dispersion	chemical reaction	liquid film diffusion	particle dispersion	chemical reaction
simultaneous equations	$y = 0.04077x + 0.17888$	$y = 0.01074x - 0.01574$	$y = 0.00795x + 0.11927$	$y = 0.12658x - 0.68793$	$y = 0.02678x - 0.15687$	$y = 0.01959x + 0.01797$
R <sup>2</sup>	0.976	0.985	0.973	0.887	0.873	0.889

adsorption of U and Mo by the resin during the dynamic adsorption process, a flow rate of 0.5 mL·min<sup>-1</sup> is used for the subsequent experiment. This flow rate was chosen to ensure that uranium and molybdenum can be fully adsorbed by the resin, thereby completing the adsorption and desorption processes.

### Dynamic adsorption and desorption experiments

Dynamic adsorption experiments were carried out to determine the adsorption and desorption effects of LSL-030-bd resin on uranium and molybdenum mixed solutions in practice. The 20 mL of LSL-030-bd resin (density 0.7 g·mL<sup>-1</sup>) was wet loaded into an ion exchange column ( $\phi \times h = 20 \text{ mm} \times 30 \text{ cm}$ ), and a peristaltic pump was used to pump the U(VI) and Mo(VI) mixed solution with a pH value of 7.0 and a concentration of 200 mg·L<sup>-1</sup> from the bottom up to the top at a flow rate of 0.5 mL·min<sup>-1</sup>, and the results are shown in the figures below Figs. 22 and 23.

Through calculation, the dynamic working adsorption capacities of uranium and molybdenum were 205.92 mg·g<sup>-1</sup> and 16.34 mg·g<sup>-1</sup>, respectively. It can be seen that Mo(VI) penetrated the earliest and basically saturated at 100 BV; U(VI) penetrated at 600 BV and basically saturated at 850 BV, and the concentration of U(VI) in the solution at this time was 173.40 mg·L<sup>-1</sup>, and the U(VI) concentration changed a lot at 650–800 BV. At 650–800 BV, the U(VI) concentration varied greatly, which was due to the slight change in pH value of uranium during the ion exchange process of the resin, resulting in the hydrolysis of U to produce precipitation, leading to the internal blockage of the resin

**Fig. 22** Dynamic adsorption of LSL-030-bd**Fig. 23** Dynamic desorption of LSL-030-bd

and making the adsorption inhomogeneous and incomplete [26]. In the range of 100–500 BV, the adsorption of Mo(VI) by LSL-030-bd resin was saturated, while there was a better adsorption of U(VI), so that the separation of Mo(VI) and U(VI) could be achieved. In the desorption experiments,  $0.1 \text{ mol}\cdot\text{L}^{-1}$   $\text{NH}_4\text{SCN}$  was used for continuous desorption. The maximum concentration of U(VI) in the desorbed solution was  $1.42 \text{ g}\cdot\text{L}^{-1}$ , and the concentration of Mo(VI) was  $0.59 \text{ g}\cdot\text{L}^{-1}$ .

## Conclusions

To sum up, the findings presented in this research can be summarized as follows:

1. The homogeneous styrenic pyridine resin (LSL-030-bd) was successfully synthesized.
2. The resin has a certain adsorption capability for both uranium and molybdenum. At a pH of 7.0, the resin achieves a maximum separation coefficient of 9.04 for uranium and molybdenum.
3. The resin's adsorption mechanism for uranium is ion exchange, while the adsorption of molybdenum is due to a chemical reaction involving hydrogen bonding. Different desorption reagents can be applied to desorb the uranium and molybdenum adsorbed by the resin in steps.

In summary, based on the findings of both static and dynamic tests, it can be concluded that the resin has the potential to simultaneously adsorb uranium and molybdenum, as well as certain industrial application prospects for the separation of uranium and molybdenum in neutral ground leach uranium extraction.

**Acknowledgements** This project was mainly supported by the China Uranium Industry Co., Ltd.- the Foundation of State Key Laboratory of Nuclear Resources and Environment Joint Innovation Fund Project (2022NRE-LH-15), Key Project of Jiangxi Natural Science Foundation (20232ACB203014) and Project of Nuclear Technology R&D Program (Proto-Nuclear Energy Development) (HNKF202311(48)).

## Declarations

**Conflict of interest** We declare that we have no known competing financial interests or personal relationships that could have appeared to influence the work reported in this paper.

## References

1. Zhao K, Li G, Zhou Y, Xu L, Liu Y, Sun Z, Zhang W, Ni F, Zhang W (2019) Research progress of leaching of sandstone-type uranium ore. *Nonferrous Metals (Extr Metall)* 06:40–48
2. Shamim A, Xiao Y, Franco P (2017) Sandstone type uranium deposits in the ordos basin, Northwest China: a case study and an overview. *J Asian Earth Sci* 146:367–382
3. Li Q (2015) Mining technical progress and development direction of low grade hard rock uranium deposit. *Uranium Min Metall* 34(02):72–77
4. Xing H, Liu Y, Chen G, Gao R, Tian S (2006) Multipurpose recovery techniques of uranium-molybdenum intergrown ores at abroad. *Uranium Min Metall* 25(04):186–191
5. Lei X, Qi G, Sun Y, Xu H, Wang Y (2014) Removal of uranium and gross radioactivity from coal bottom ash by  $\text{CaCl}_2$  roasting followed by  $\text{HNO}_3$  leaching. *J Hazard* 276:346–352
6. Liu K, Yang Z, Liu Y, Ma J, Shi L, Li W, Yang J, Gao D, Zhang Y (2017) Study on occurrence modes and leaching performance of a uranium-molybdenum associated ore. *Uranium Min Metall* 36(02):93–98
7. Zhang H, Li H, Liang J, Zhang L (2020) Current status and progress of rare metal molybdenum resource recovery. *Multipurp Util Miner Resour* 01:47–49
8. Zhao H, Ning Y, Wang W, Zhang B, Liu H, Ren Z (2018) Experimental study on adsorption of molybdenum by D314 resin. *Min Metall Eng* 38(1):81–83
9. Lasheen TA, El-Ahmady ME, Hassib HB, Helal AS (2015) Molybdenum metallurgy review: hydrometallurgical routes to recovery of molybdenum from ores and mineral raw materials. *Miner Process Extr M* 36(03):145–173
10. Selvan B, Suneesh A, Ramanathan N (2023) Diglycolamic acid coated cation exchange adsorbent for uranium removal by extraction chromatography. *J Radioanal Nucl Chem* 332:1775–1786
11. Zhao J (2022) Genesis analysis of Yangluozigou uranium-molybdenum deposit in Longhua County. Hebei CEO University, Hebei
12. Wang L, Zhou X, Tang L (2015) Study on recycling Mo from the acidic waste water by ionexchange resin. *China Molybd Ind* 4:48–49
13. Guo S (2015) Recovery of molybdenum from molybdenum precipitation solution by D314 Ion-exchange resin. *Hydrometallurgy* 06:471–473
14. Orrego P, Hernández J, Reyes A (2019) Uranium and molybdenum recovery from copper leaching solutions using ion exchange. *Hydrometallurgy* 184:116–122
15. Smedley PL, Kinniburgh DG (2023) Uranium in natural waters and the environment: distribution, speciation and impact. *Appl Geochem* 148:1055345
16. Ma T (2016) Studies on extraction of U(VI) by picolinamide. East China University of Technology, Nanchang
17. Chen Y (2018) Treatment of desulfurization wastewater by in situ synthesis of LDH. North China Electric Power University, Beijing
18. Liu F (2020) Synthesis of two N-type adsorption materials and their application in recovery of rhenium from leaching. East China University of Technology, Nanchang
19. Xiao Z, Zhang Z, Pan X, Liu Y, Zheng Z, Wang Y (2019) Adsorption of U(VI) in aqueous solution by magnetic manganese dioxide. *Hydrometallurgy* 38(03):195–201
20. Wang QL (2009) Uranium extraction technology. Harbin Engineering University Press, Harbin
21. Triki M, Tanazefi H, Kochkar H (2017) Design of  $\beta$ -cyclodextrin modified  $\text{TiO}_2$  nanotubes for the adsorption of Cu(II): Isotherms and kinetics study. *J Colloid Interface Sci* 493:77–84
22. Yu Y, Wan Q (2023) Adsorption of uranium (VI) in aqueous solutions by phosphorylated adsorbent resin porous carbon. *J Radioanal Nucl Chem* 332:4201–4211. <https://doi.org/10.1007/s10967-023-09093-y>
23. Wang L (2020) Studies on removal of heavy metals and antibiotics by pyridine-functionalized chitosan adsorbents. Hainan Normal University, Haikou

24. Wu X, Liu H, Wang R, Jiang H (2015) The effect of initial concentration and pH value of the uranyl nitrate solution on the its hydrolysis reaction. *J Liaoning Petrochem Univ* 35(05):18–21
25. Xiu T, Zhang M, Ye G, Jiao G, Yuan L, Shi W (2023) The study on the extraction separation and mechanism of U(VI)/Mo(VI) by bipyridine diamide ligands. *J Harbin Eng Univ* 44(12):2177–2184
26. Zhao W (2018) Studies on synthesis of hydrothermal carbon microspheres from lignin by template method and the adsorption properties of uranium. Southwest University of Science and Technology, Mianyang

**Publisher's Note** Springer Nature remains neutral with regard to jurisdictional claims in published maps and institutional affiliations.

Springer Nature or its licensor (e.g. a society or other partner) holds exclusive rights to this article under a publishing agreement with the author(s) or other rightsholder(s); author self-archiving of the accepted manuscript version of this article is solely governed by the terms of such publishing agreement and applicable law.